

Research on Engineering Structures & Materials



www.jresm.org



Numerical analysis of the impact of PCM reservoir width on lithium-ion battery cooling: A constructal design study

Rafael da Silveira Borahel, Giovani Dambros Telli, Augusto Antoniolli Bolzoni, Liércio André Isoldi, Elizaldo Domingues dos Santos, Luiz Alberto Oliveira Rocha

Online Publication Date: 30 February 2025

URL: http://www.jresm.org/archive/resm2025-557en1202rs.html

DOI: http://dx.doi.org/10.17515/resm2025-557en1202rs

Journal Abbreviation: Res. Eng. Struct. Mater.

To cite this article

Borahel R D S, Telli G D, Bolzoni A A, Isoldi L A, dos Santos E D, Luiz Rocha A O. Numerical analysis of the impact of PCM reservoir width on lithium-ion battery cooling: A constructal design study. *Res. Eng. Struct. Mater.*, 2025; 11(5): 2421-2435.

Disclaimer

All the opinions and statements expressed in the papers are on the responsibility of author(s) and are not to be regarded as those of the journal of Research on Engineering Structures and Materials (RESM) organization or related parties. The publishers make no warranty, explicit or implied, or make any representation with respect to the contents of any article will be complete or accurate or up to date. The accuracy of any instructions, equations, or other information should be independently verified. The publisher and related parties shall not be liable for any loss, actions, claims, proceedings, demand or costs or damages whatsoever or howsoever caused arising directly or indirectly in connection with use of the information given in the journal or related means.



Published articles are freely available to users under the terms of Creative Commons Attribution - NonCommercial 4.0 International Public License, as currently displayed at here (the "CC BY - NC").



Research on Engineering Structures & Materials



www.jresm.org

Research Article

Numerical analysis of the impact of PCM reservoir width on lithium-ion battery cooling: A constructal design study

Rafael da Silveira Borahel ^{1,a}, Giovani Dambros Telli ^{2,b}, Augusto Antoniolli Bolzoni ^{2,c}, Liércio André Isoldi ^{1,d}, Elizaldo Domingues dos Santos ^{1,e},Luiz Alberto Oliveira Rocha*,^{1,3,4,f}

- ¹School of Engineering, Federal University of Rio Grande, Brazil
- ²University of Caxias do Sul, Brazil
- ${\it ^3Graduate\ Program\ of\ Mechanical\ Engineering\ (PROMEC),\ Federal\ University\ of\ Rio\ Grande\ do\ Sul,\ Brazil}$
- ⁴Institute of Earth Sciences, Complex Fluid Systems Lab, Portugal

Article Info Abstract The aim of this work is to examine, from the perspective of Constructal Design, Article history: the influence of the width (W_{pcm}) of a reservoir filled with PCM (phase change material) on the cooling performance of a Li-ion battery cell under discharge Received 02 Dec 2024 rates of 3C and 5C. The problem is considered two-dimensional and transient. Accepted 25 Feb 2025 The mathematical model is multiphase, with different characteristics for the solid domain (battery cell) and the fluid domain (PCM reservoir), based on the Keywords: mass, momentum and energy balance equations. The finite volume method is used to solve the problem numerically, and the grid meshes used in the spatial Constructal design; discretization are subjected to uncertainty analysis. The results show that the Lithium-Ion battery; use of the PCM reservoir contributes significantly to the cooling of the battery. Battery cooling; When the battery discharge occurs at a rate of 5C, there is a 13.1°C reduction in Thermal runaway the maximum temperature of the battery (T_{max}) .

© 2025 MIM Research Group. All rights reserved.

1. Introduction

Never in history has there been a more urgent need to reassess the impact of our society on the planet, especially with regard to climate change caused by the carbon emissions from our activities. Internal combustion engine vehicles are one of the largest contributors to global pollution, with the transportation sector accounting for approximately 20% of the world's total carbon emissions [1,2]. However, this scenario is about to change as government policies focused on promoting electric vehicles (EVs) gain momentum. In the European Union (EU), for example, only non-CO₂-emitting vehicles, such as EVs, will be permitted to be registered in member countries from 2035 [3]. To achieve this goal, automakers are redoubling their efforts to improve their EVs, with a particular focus on developing the battery packs that will power them.

Lithium-ion (Li-ion) batteries are the best-known power source for electric vehicles due to their high energy and power density, no memory effect, long cycle life, and fast charging capability [4,5]. Despite these advantages, Li-ion batteries require strict thermal control to ensure their performance and safety. In general, very low temperatures increase the battery's internal resistance and polarization, resulting in higher power and energy losses and reduced discharge capacity. On the other hand, very high temperatures accelerate battery degradation, reducing its performance, lifespan and security [6]. According to

DOI: http://dx.doi.org/10.17515/resm2025-557en1202rs

^{*}Corresponding author: luizrocha@mecanica.ufrgs.br

^a orcid.org/0000-0002-8724-132x; ^b orcid.org/0000-0003-1294-0668; ^c orcid.org/0009-0005-7608-6773;

dorcid.org/0000-0002-9337-3169; corcid.org/0000-0003-4566-2350; forcid.org/0000-0003-2409-3152

Pesaran [7], the ideal operating temperature for Li-ion batteries is between 25 and 40°C, with the temperature variation within each cell not exceeding 5°C.

Battery thermal management systems (BTMS) are divided into three main categories: active, passive, and hybrid [8]. Passive BTMS based on phase change materials (PCMs) have gained popularity due to their lower complexity, cost and volume; in addition to offering a more uniform battery cooling [9,10]. Srivastava et al. [11] studied the cooling of a cylindrical Li-ion battery surrounded by PCMs. The results obtained show that the use of PCMs is a viable approach to reduce the maximum temperature reached by the battery. Alghassab [12] evaluated the potential of a finned BTMS based on PCM to improve the thermal management of a Li-ion battery. With six copper fins, the authors found an 8°C reduction in battery peak temperature. In both studies, the geometric parameters of the PCM container showed a significant role on the battery cooling. Therefore, adequate thermal control of the battery depends on the correct design of the PCM reservoir, whose geometry can be developed using the Constructal Design Method (CDM).

The CDM has its origins in constructal theory, which supports the idea that the configuration/evolution of any flow system - animated or not - occurs through a physical principle, the constructal law [13,14]. In the constructal realm, the design of the flow system evolves in such way to easily the internal currents, including the engineering systems, where the Constructal Law is applied through the CDM [15]. In engineering, this method has been used to study the geometry of a wide variety of finite-size flow systems [16-19]. It can even be applied to the analysis of the design of passive PCM-based BTMS in Li-ion battery packs, which have a limited volume in EVs. Therefore, the aim of this numerical study is to analyze, using the Constructal Design Method (CDM), the effect of the width of a PCM reservoir (W_{PCM}) on the cooling performance of a Li-ion battery pack discharged at rates of 3C and 5C.

2. Methodology

2.1. Constructal Design Method (CDM)

The geometry of the proposed BTMS was studied using the Constructal Design Method (CDM). The CDM is a method based on constraints (geometric and physical) and objectives (performance indicators), organized in a sequence of well-defined steps [17-20] that are outlined below and illustrated in the flowchart shown in Figure 1.

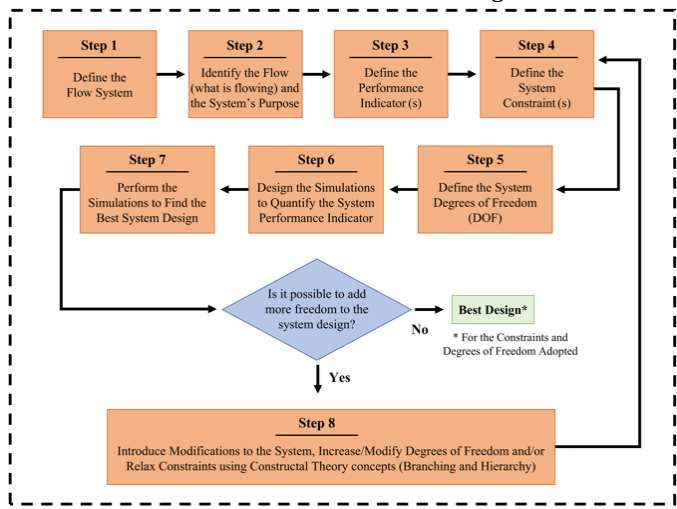


Fig. 1. Flowchart of steps involved in applying the Constructal Design Method (CDM)

Step 1: Define the Flow System

The system under analysis consists of a Li-ion battery pack $[\text{Li}(\text{Ni}_1/_3\text{Co}_1/_3\text{Mn}_1/_3)\text{O}_2]$ composed of six battery cells connected in a 3s2p configuration by a copper busbar. The battery pack is exposed to ambient air ($T_\infty = 25\,^{\circ}\text{C}$) and dissipates heat to it by natural convection with a convection heat transfer coefficient (h) equal to 12.8 W/m²K [21]. The battery cells are 148.8 mm in length (L_{cell}) and 91.6 mm in height (H_{cell}), with a width (W_{cell}) of 26.8 mm. Between each pair of cells, two thermal reservoirs filled with PCM (RT 28HC) are placed, with a thin layer of insulation separating them. The PCM reservoirs are the same length (L_{pcm}) and height (H_{pcm}) as the battery cells, while their width (W_{pcm}) is variable to assess their effects on battery cooling. This analysis is conducted using ϕ , which is defined as the ratio between W_{pcm} and W_{cell} .

The schematic representation of the battery pack analyzed is shown in Fig. 2 (a-c); where Fig. 2 (a) presents the isometric view of the battery pack, Fig. 2 (b) the side view, with the red dashed line delineating the computational domain adopted, which is shown in Fig. 2 (c) with the applied boundary conditions. For clarity, the computational domain consists of a cross-sectional cut of the battery pack, covering (for computational economy) only half of one of the central battery cells and the adjacent PCM reservoir.

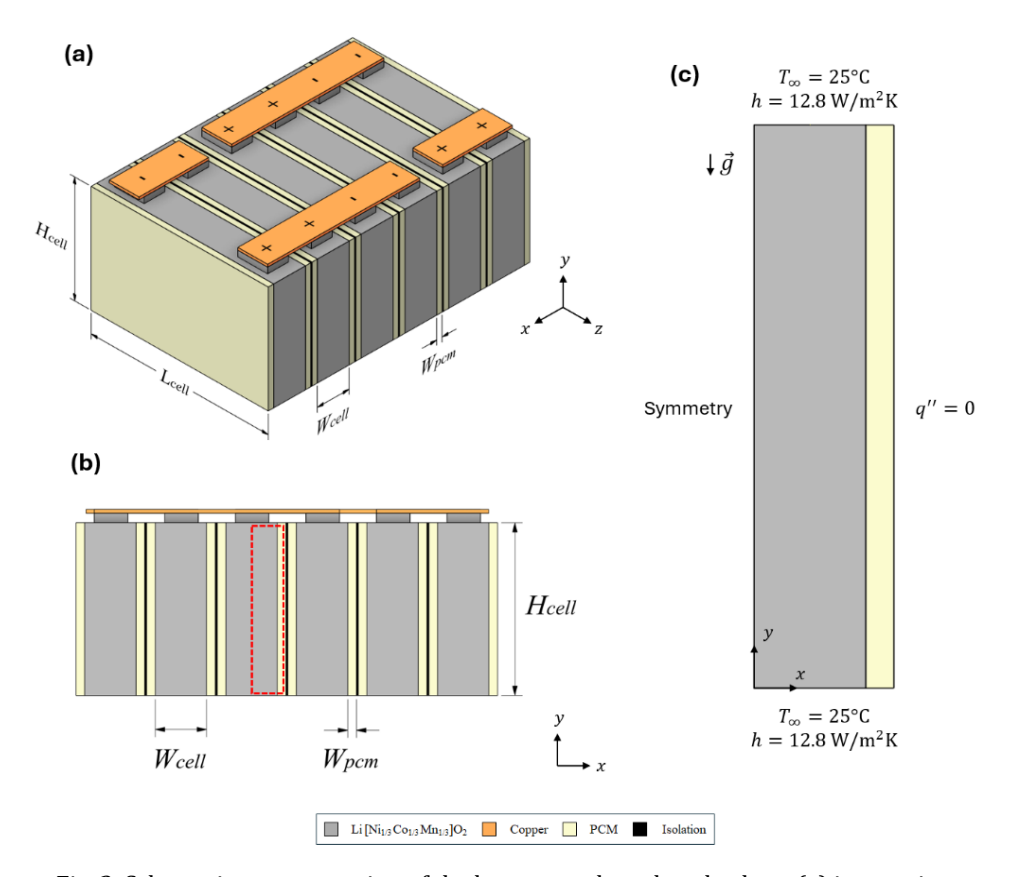


Fig. 2. Schematic representation of the battery pack analyzed, where (a) isometric view, (b) side view and (c) computational domain adopted

The technical specifications and physical properties of the battery cells and the copper busbar are shown in Table 1, while the properties of the PCM (RT 28HC) are shown in Table 2. Since the thermal conductivity of battery cells (k_{cell}) has an anisotropic behavior, three values are presented for this property, valid for the x, y, and z axes, respectively.

Table 1. Physical properties and technical specifications of the battery cells and busbar.

Physical Properties	Battery Cell [22] Cooper Busbar [23	
Density (ρ)	2630 (kg/m ³)	8978 (kg/m ³)
Specific Heat Capacity (c_p)	1100 (J/kg. K)	381 (J/kg. K)
Thermal Conductivity (k)	22.4; 22.4; 1.96 (W/m. K)	387.6 (W/m. K)
Nominal Capacity	37 (Ah)	X - X - X - X - X
Nominal Voltage	3.7 (V)	X - X - X - X - X
Operation Voltage	2.8 – 4.2 (V)	X - X - X - X - X

Table 2. Physical properties of the PCM (RT 28HC)

Physical Properties	RT 28HC [24-25]
Density (ρ)	880 (kg/m³) at 15°C; 770 (kg/m³) at 40°C
Latent Heat (Q_{lat})	250000 (J/kg)
Specific Heat Capacity (c_p)	2000 (J/kg. K)
Thermal Conductivity (k)	0.2 (W/m. K)
Thermal Expansion Coefficient (β)	0.001 (1/K)
Viscosity (μ)	0.0031 (kg/m.s)
Liquidus Temperature (T_L)	29°C
Solidus Temperature (T_S)	27°C

• Step 2: Identify the Flow (*what is flowing*) and the System's Purpose

The purpose of the BTMS evaluated is to promote the cooling of the battery cell. Thus, from the Constructal Theory perspective, the "flow" in this system corresponds to the heat generated by the battery, which is dissipated to the ambient air and the PCM reservoir.

• Step 3: Define the System Performance Indicators

As the purpose of the system is to promote the thermal management of the battery, the performance indicators are the maximum battery temperature (T_{max}) and its temperature difference ($\Delta T_{cell} = T_{max} - T_{min}$) for each instant of time, which reflects the cooling uniformity.

• Step 4: Define the System Constraints

In the proposed problem, the only system constraint is the battery cell volume (V_{cell}), given by:

$$V_{cell} = (L.H.W)_{cell} \tag{1}$$

Step 5: Define the System Degrees of Freedom (DoF)

The degree of freedom (DoF) admitted for the system is the PCM reservoir width (W_{pcm}), which is expressed in its dimensionless form as:

$$\phi = \frac{W_{pcm}}{W_{cell}} \tag{2}$$

where ϕ is the ratio between the PCM reservoir and battery cell volumes (V_{pcm} and V_{cell}), which in a simplified form gives the width fraction shown in Eq. (2).

• Step 6: Define the Simulations to Quantify the System Performance Indicators

The simulations necessary to evaluate the variations of T_{max} and ΔT_{cell} in response to the system's DoF were designed considering four values to ϕ (0.05, 0.10, 0.15, 0.20) and two battery discharge rates (3C and 5C), resulting in 8 different cases analyzed.

• Step 7: Perform the Simulations to Find the Best System Design

The proposed problem was solved computationally using numerical simulations based on the Finite Volume Method (FVM), performed in the software ANSYS FLUENT 2023 R1.

 Step 8: Introducing Modifications on the System (Increasing DOF/Relaxing Restrictions)

The increase in the system's DoF or the relaxation of its constraints drives the evolution of its design, facilitating the "flow" (the heat generated by the battery) and enhancing the overall system performance. In this work, this step in the application of the CDM was not taken; however, it could be implemented in future works with the purpose of further minimizing the predefined performance indicators (T_{max} and ΔT_{cell}).

2.2. Mathematical Model

The proposed problem is considered two-dimensional and transient. The mathematical model is multiphase, with different characteristics for the solid domain (battery cell) and the fluid domain (PCM reservoir).

2.2.1 Solid Domain (Battery Cell)

The mathematical model implemented for the solid domain (battery cell) consists only of the energy conservation equation [26]:

$$\frac{\partial}{\partial t} (\rho c_p T) = \nabla (k \nabla T) + \dot{q}^{\prime \prime \prime} \tag{3}$$

where t is the time, T is the temperature and \dot{q}''' is the battery volumetric heat generation rate, whose variation with time for the 3C and 5C discharge rates are given by the polynomial equations (3) and (4). These are taken from a previous work [27], that first modeled the battery discharge process, and consequently its heating, using the equivalent circuit model (ECM) [28-29]. The data obtained was then used by the authors to generate the polynomial equations to model the battery heating in terms of \dot{q}''' , which proved to be as effective as the ECM, but requiring less computational time [27].

$$\dot{q}_{(3C)}^{\prime\prime\prime} = 2.244e^{-14}(t^6) + 1.264e^{-9}(t^5) - 3.677e^{-6}(t^4) + 3.096e^{-3}(t^3)$$

$$-1.926t^2 + 471.71t + 34977.73$$

$$\dot{q}_{(5C)}^{\prime\prime\prime} = -1.559e^{-11}(t^6) + 6.683e^{-8}(t^5) - 8.526e^{-5}(t^4) + 0.0482e(t^3)$$
(5)

$$\dot{q}_{(5C)}^{\prime\prime\prime} = -1.559e^{-11}(t^6) + 6.683e^{-8}(t^5) - 8.526e^{-5}(t^4) + 0.0482e(t^3)$$

$$-13.36t^2 + 1876.77t + 65130.84$$
(5)

2.2.2 Fluid Domain (PCM Reservoir)

The flow of the liquid PCM is considered Newtonian, laminar, and incompressible. The mathematical model implemented in the fluid domain is based on the conservation equations of mass, energy and momentum, supplemented by the enthalpy-porosity method used to model the PCM melting [28].

$$\nabla(\rho\vec{V}) = 0 \tag{6}$$

$$\frac{\partial(\rho\lambda)}{\partial t} + \nabla(\rho\vec{V}\lambda) = \nabla(k\nabla T) \tag{7}$$

$$\frac{\partial \rho \vec{V}}{\partial t} + \nabla (\rho \vec{V} \vec{V}) = -\nabla p + \nabla (\mu \nabla \vec{V}) + \rho \vec{g} + \vec{S}$$
(8)

where \vec{V} is the velocity vector, λ is the total specific enthalpy, p is the pressure, \vec{g} is the gravity acceleration and \vec{S} is the momentum source term, given by:

$$\vec{S} = -A_{(x)} \cdot \vec{V} \tag{9}$$

where $A_{(\gamma)}$ is the porosity function, which is defined by Voller and Prakash [30] as follows:

$$A = \frac{C(1-\gamma)^2}{(\gamma^3 + \omega)} \tag{10}$$

where C is the mushy zone constant, whose value in this study is equal to 10^6 [31]; ω is a small constant (0.001) to avoid division by zero and γ is the PCM liquid fraction, determined by:

$$\gamma = \begin{cases}
0 & if & T < T_s \\
\frac{T - T_s}{T_l - T_s} & if & T_s < T < T_l \\
1 & if & T > T_l
\end{cases}$$
(11)

Finally, the PCM total specific enthalpy (λ) is the sum of its sensible (λ_{sen}) and latent (λ_{lat}) specific enthalpies:

$$\lambda = \lambda_{sen} + \lambda_{lat} \tag{12}$$

where λ_{sen} and λ_{lat} are defined as follows, respectively:

$$\lambda_{sen} = \lambda_{ref} + \int_{T_{ref}}^{T} c_p dt \tag{13}$$

$$\lambda_{lat} = \begin{cases} 0 & if & T < T_s \\ \gamma Q_{lat} & if & T_s < T < T_l \\ Q_{lat} & if & T > T_l \end{cases}$$

$$(14)$$

where λ_{ref} is the reference specific enthalpy at a reference temperature (T_{ref}) .

2.2.3 Initial and Boundary Conditions

As previously shown in Fig. 2 (c), three different types of boundary conditions were implemented in the computational domain. At the top and bottom walls of the battery cell and the PCM reservoir, heat dissipation by natural convection to the environment was considered, with a convection heat transfer coefficient (h) equal to 12.8 W/m²K and an ambient temperature (T_{∞}) of 25°C. The symmetry condition was applied to the left wall, while the right wall was considered thermally isolated, assuming a null heat flux (q''=0). Finally, as an initial condition, the initial temperature (T_i) of the computational domain was assumed equal to 25°C.

2.3. Numerical Model

The proposed problem was solved computationally through numerical simulations in ANSYS Fluent 2023 R1, a computational fluid dynamics (CFD) software based on the FVM. SIMPLE scheme was used to handle the pressure-velocity coupling, *Least Squares Cell-Based* was applied for spatial discretization of gradients, and PRESTO! scheme for pressure. Finally, the *Second Order Upwind* method was used for momentum and energy equations terms. Residuals of 10^{-3} were adopted as the convergence criterion for the continuity and

momentum equations, while 10^{-6} was applied for energy. For the time discretization, three-time steps (0.01s, 0.05s, and 0.1s) were tested and the difference between them for the discharge rate of 5C was analyzed in terms of T_{min} and T_{max} as a function of the battery State of Charge (SoC) for the $\phi = 0.10$ case, as shown in Fig. 3 (a-b).

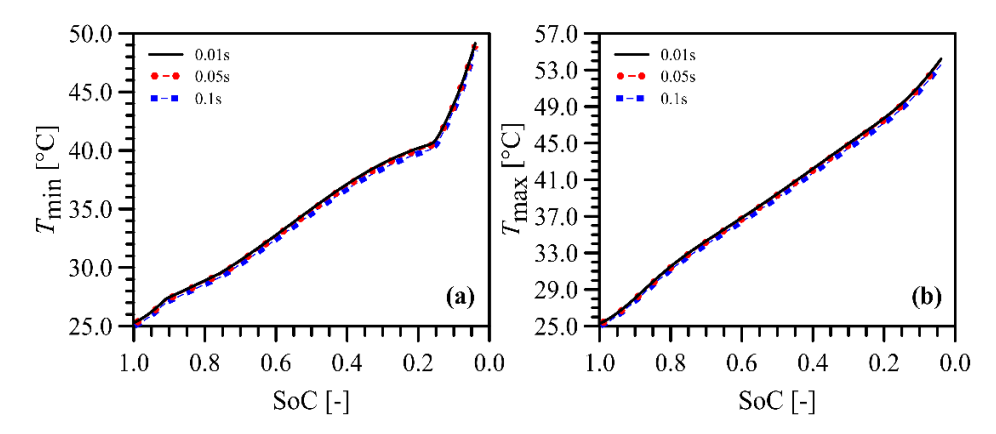


Fig. 3. Minimum and maximum temperatures of the battery as a function of its state of charge (SoC) for the discharge rate of 5C and $\phi = 0.10$, with the three-time steps tested: 0.01s, 0.05s, and 0.1s

As can be seen in Fig. 3 (a-b), the difference between the results obtained with the different time steps is minimal, which indicates that any of the values tested are adequate. In the present work, the intermediate value has been chosen due to the more stable solution obtained with it, which required fewer iterations for the convergence of the equations and, consequently, a shorter computational time. Therefore, a time step of 0.05s was chosen for all simulations, with a maximum of 1000 iterations per time interval, resulting in a computational time of 12 to 48 hours per simulation.

Table 3. Uncertainty between meshes M1 and M2 (GCI₂₁) and M2 and M3 (GCI₃₂)

Performance Indicators	GCI ₂₁	GCI ₃₂
Battery Maximum Temperature (T_{max})	0.03%	0.09%
Battery Difference Temperature (ΔT_{cell})	0.07%	0.12%

The spatial discretization of the computational domain was carried out using structured grid meshes composed of square cells. A higher density of cells was applied along the battery cell/PCM reservoir interface, as well as on all the solid walls of the PCM reservoir, refining the regions where the largest temperature and velocity gradients occur. The mesh uncertainty analysis was conducted using the *Grid Convergence Index* (GCI) method [32-33]. For this purpose, three grid meshes with different numbers of cells (91350, 63945, and 44742 cells; referred to as M1, M2, and M3, respectively) were created and tested in the computational domain. Table 3 shows the uncertainty between meshes M1 and M2 (GCI₂₁), as well as between meshes M2 and M3 (GCI₃₂), for T_{max} and ΔT_{cell} at the end of the battery discharge process (SoC = 0), calculated for the case in which the discharge rate is equal to 5C and ϕ = 0.10. As can be observed, for both performance indicators analyzed, GCI₂₁ and GCI₃₂ were found to be below 1%, indicating that the results are not dependent on the meshes. Therefore, the most refined grid mesh – containing 91350 cells – is appropriate for the spatial discretization of the

computational domain; thus, all the other grid meshes were built based on the construction parameters of the respective mesh.

2.4. Model Verification

In order to verify that the mathematical and numerical models implemented are indeed appropriate for the proposed study, initially they were employed to reproduce a similar. study from the literature. The study reproduced for this purpose was the numerical work by Borahel *et al.* [27], which investigated the discharge process of a Li-ion battery pack with the same technical specifications and assembly scheme as the battery studied in this paper. The main difference between the works is the complexity of the models implemented, as Borahel *et al.* [27] evaluate the battery as a whole, in three dimensions, including the electrical effects of discharge through the Equivalent Circuit Model (ECM) [32-33]. Furthermore, in the reference work, the battery is cooled exclusively by natural convection, without the PCM reservoirs between the battery cells, as in the present study.

Fig. 4 (a-b) shows the battery temperature as a function of its State of Charge (SoC) for the discharge rates of 3C and 5C, based on the results reported by Borahel *et al.* [27] and present work; where (a) display the battery average temperature (T_{ave}) and (b) the maximum temperature (T_{max}).

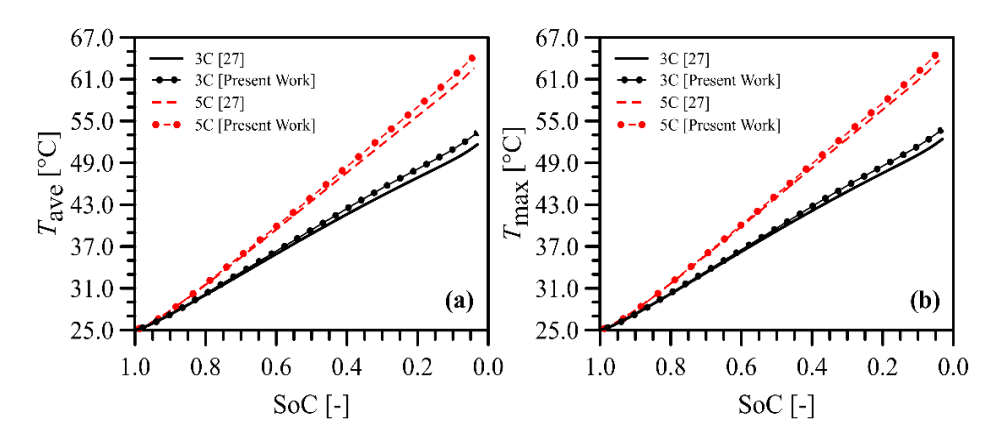
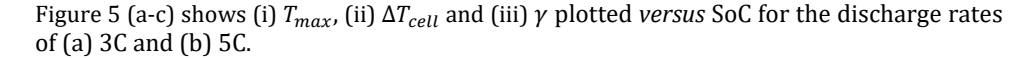


Fig. 4. Average and maximum battery temperatures as a function of State of Charge (SoC) for the discharge rates of 3C and 5C, obtained by Borahel *et al.* [27] and the present work

As can be seen in Fig. 4 (a-b), the results obtained using the mathematical and numerical models implemented in this work are very similar to those reported by Borahel $et\ al.\ [27]$ for both discharge rates tested. The maximum difference observed between the results in terms of T_{ave} [Fig. 4(a)] was 1.68°C for the 3C discharge rate and 1.74°C for 5C, both found at the end of the discharge process. Regarding T_{max} [Fig. 4(b)], the maximum differences were equals to 1.40°C and 1.32°C for 3C and 5C discharge rates, respectively. Therefore, despite being significantly simpler than the models used by Borahel $et\ al.\ [27]$, the models implemented in this study were also able to adequately reproduce the heating of the Li-ion battery pack during its discharge. Thus, it can be said that the implemented models are indeed suitable for the proposed study.

3. Results and Discussion

For both discharge rates used (3C and 5C), the cooling of the battery cell and consequently the performance of the BTMS as a function of ϕ was evaluated in terms of T_{max} and ΔT_{cell} .



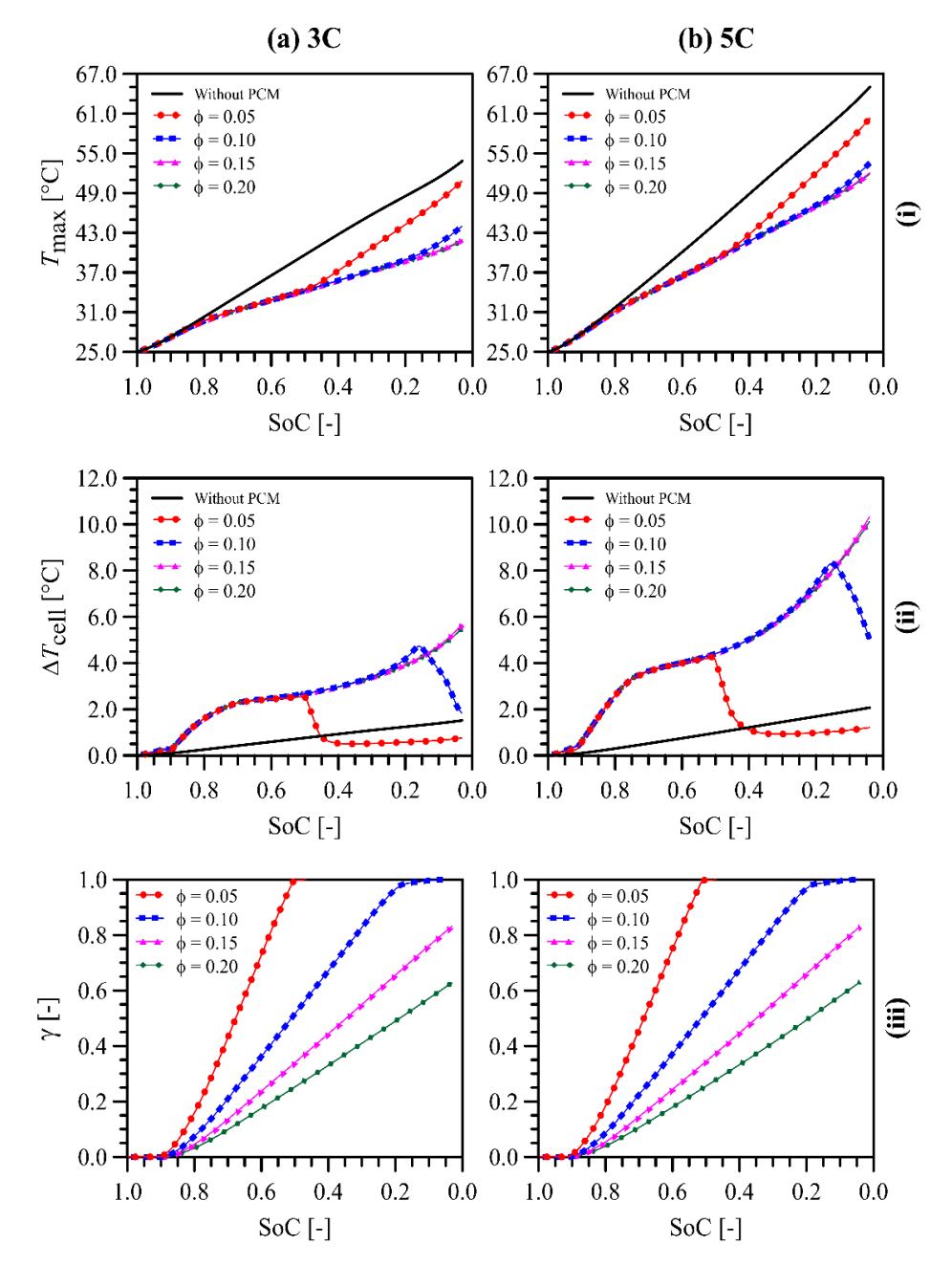


Fig. 5. Curves of (i) T_{max} , (ii) ΔT_{cell} and (iii) γ as a function of SoC for (a) 3C and (b) 5C discharge rates

In this figure, the results of the battery without BTMS are compared with those obtained for the cases with BTMS (with PCM reservoir), where W_{pcm} and, consequently, V_{pcm} , vary with ϕ .As expected, the battery cell heats up throughout the discharge, with the heating

being more pronounced in the 5C case. The highest values of T_{max} are reached at the end of the discharge (SoC \cong 0), regardless of the presence or absence of the PCM reservoir. At this stage of discharge, T_{max} was 53,8°C for the 3C case without the PCM reservoir [Fig. 5 (a)(i)], followed by 50.8°C for the $\phi = 0.05$ case; 44°C for $\phi = 0.10$; 42°C for $\phi = 0.15$ and 41.8°C for $\phi = 0.20$. For the same cases, but considering the 5C discharge rate [Fig. 5 (b)(i)], T_{max} at SoC \approx 0 were 65°C; 60.3°C; 53.6°C; 52.1°C and 51.9°C, respectively. Thus, it is clear that the PCM reservoir contributed to the battery cooling, reducing T_{max} by 12°C (53.8°C \rightarrow 41.8°C) in the 3C discharge rate cases and by 13.1°C (65°C \rightarrow 51.9°C) for 5C. Despite the significant reduction in T_{max} , its maximum values are still above the ideal operating temperature range considered in the present work, which varies between 25°C and 40°C [7]; however, it is still lower than the maximum acceptable temperature (60°C) [34] proposed by some authors and manufacturers. A more detailed analysis of the T_{max} behavior as a function of SoC shows that the battery temperature is not affected by the PCM reservoir in the early stages (SoC \geq 0.8) of the discharge process. The PCM reservoir only begins to contribute to the battery cooling after SoC = 0.8, when the battery temperature exceeds the PCM melting temperature, initiating the melting process, as shown in Fig. 5 (a-b) (iii). For all ϕ tested, T_{max} showed a very similar behavior until SoC = 0.45. After this moment, T_{max} for the $\phi = 0.05$ case has a more pronounced increase. Since W_{pcm} is reduced for $\phi = 0.05$, the PCM volume (V_{pcm}) and, consequently, the PCM mass are smaller. Thus, the PCM reservoir completes its melting more quickly, in the first half of the battery discharge process (SoC \cong 0.50), as illustrated in Fig. 5 (a-b) (iii). As a result, the battery cell loses the thermal protection provided by the PCM in the second half of the discharge process, which justifies the increase in T_{max} . For the same reason, a more pronounced heating is observed in the $\phi = 0.10$ case during the final stages of discharge [Fig. 5 (a-b) (i)], as the complete melting of the PCM occurs at $SoC \cong 0.1$. On the order hand, V_{pcm} proved to be higher than necessary in the $\phi=0.15$ and 0.2 cases. Thus, at the end of the discharge process, there is still unmelted PCM in the reservoir [Fig. 5 (a-b) (iii)], which explains the great similarity of T_{max} between these two cases.

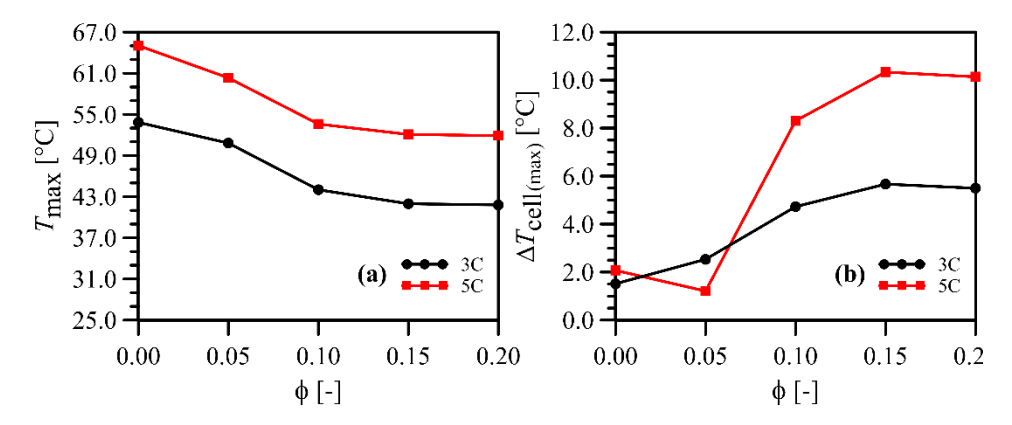


Fig. 6. Curves of (a) T_{max} and (b) $\Delta T_{cell(max)}$ as a function of ϕ for the discharge rates of 3C and 5C

The PCM reservoir, and consequently the ϕ value, also had a significant influence on ΔT_{cell} . This is illustrated in Fig. 5 (a-b)(ii), which presents the variation of ΔT_{cell} as a function of SoC for the battery cell without PCM reservoir, as well as for the cases with reservoir and different ϕ values. For both discharge rates (3C and 5C), the lowest ΔT_{cell} values are associated with the baseline cases (without PCM). When the PCM reservoir is included, there is an increase in ΔT_{cell} , which shows that the cooling it provides is not uniform, especially for the highest values of ϕ . For $\phi=0.05$ and 0.10, ΔT_{cell} exhibits an increasing

behavior identical to that observed for $\phi=0.15$ and 0.20. However, after the PCM has melted completely, ΔT_{cell} decreases rapidly, suggesting that the battery cell temperature becomes more uniform as the PCM reservoir ceases to contribute to its cooling. Figure 6 (a-b) provides a more detailed view of the effects of ϕ on the battery cell cooling, showing (a) T_{max} and (b) the maximum cell temperature difference ($\Delta T_{cell(max)}$) as a function of ϕ for the discharge rates of 3C and 5C.

As can be seen in Fig. 6 (a-b), T_{max} and $\Delta T_{cell(max)}$ show opposite behaviors with respect to ϕ . While T_{max} decreases with ϕ for both discharge rates, $\Delta T_{cell(max)}$ increases. This indicates that increasing the PCM volume by ϕ , and therefore its mass, helps to reduce the battery temperature, but the cooling is not homogeneous, as already mentioned. However, ϕ ceases to affect T_{max} and $\Delta T_{cell(max)}$ when its value exceeds 0.1; as evidenced by the nearly constant behavior of these variables for $\phi > 0.1$. This means that it is not necessary to continuously increase the volume of the PCM reservoir to further reduce T_{max} so that its maximum value does not exceed 40°C or to ensure that $\Delta T_{cell(max)}$ does not exceed 5°C. Instead, it requires ensuring that the PCM melts completely at the right time (end of discharge) and that the heat generated by the battery is dissipated homogeneously, which was not achieved for $\phi = 0.15$ and 0.20.

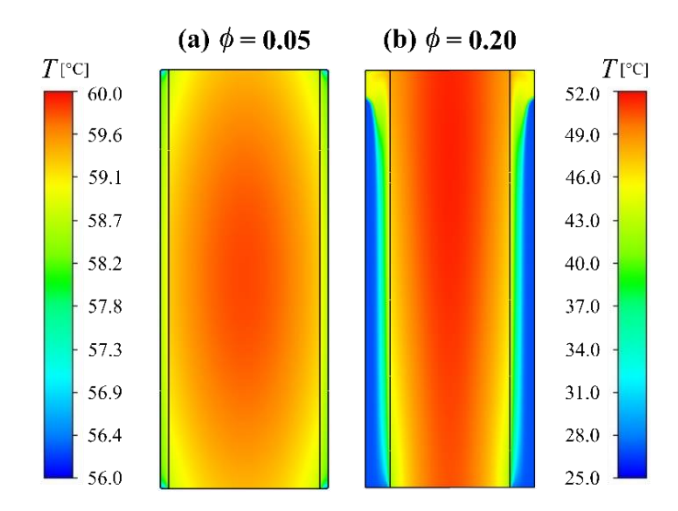


Fig. 7. Temperature contours of the battery cell and the PCM reservoir at the end of the discharge process (SoC \cong 0) for the 5C rate, where: (a) $\phi = 0.05$ and (b) $\phi = 0.20$

Figure 7 (a-b) presents the temperature contours of the battery cell and the PCM reservoir at the end of the discharge process (SoC \cong 0) for the 5C rate, considering (a) ϕ = 0.05 and (b) ϕ = 0.20. As shown in Fig. 7 (a-b), the highest battery temperatures are concentrated in the center of the cell, regardless of ϕ . The battery temperatures are higher in the case with ϕ = 0.05 compared to the case with ϕ = 0.20, as previously indicated by Fig. 5 (b)(i) and 6 (a). Analyzing the PCM reservoir for the case with ϕ = 0.05 [Fig. 6 (a)], it is clearly visible a homogeneous temperature that varies in a range of values between 58 and 59°C, which is much higher than the PCM melting temperature, 29°C. Therefore, the PCM is entirely liquefied, consistent with what is shown in Fig. 5 (b)(iii). On the other hand, the PCM reservoir for the case with ϕ = 0.20 [Fig. 7 (b)] shows heterogeneous temperatures, ranging from 25°C to approximately 49°C at its top. The dark blue areas indicate temperatures below the PCM melting temperature, meaning the PCM is still in its solid phase. Thus, the silhouette of the solid layer is clearly visible, being thicker at the base of

the reservoir and gradually thinning towards the top. This shape of the solid PCM layer is closely related to the convection mechanism, which generates an ascending plume of liquid PCM. This liquid PCM accumulates at the top of the reservoir, and due to its higher temperatures, it erodes the solid PCM layer. This accumulation of liquid PCM with higher temperatures at the top of the reservoir is detrimental to the battery cooling, because it reduces the heat dissipation and creates temperature gradients between the top and bottom regions of the battery cell.

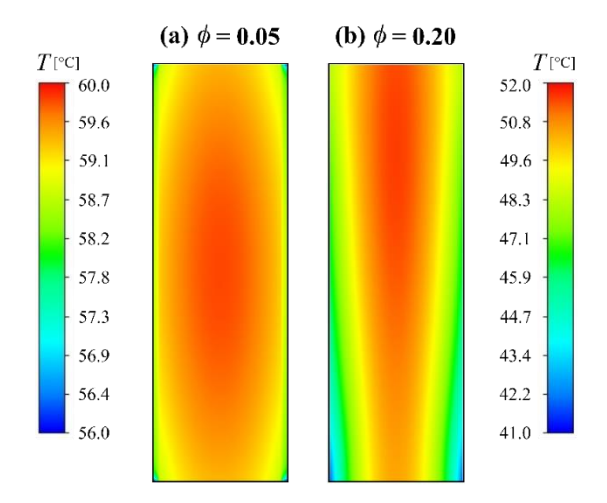


Fig. 8. Temperature contours of the battery cell at the end of its discharge process (SoC \cong 0) for the 5C rate, with (a) $\phi = 0.05$ and (b) $\phi = 0.20$

A better understanding of how the natural convection of the liquid PCM affects the temperature distribution of the battery cell is provided by Figure 8 (a-b), which shows the temperature contours of the battery at the end of its discharge process (SoC \cong 0) for the 5C rate, with (a) $\phi = 0.05$ and (b) $\phi = 0.20$. This figure differs from Fig. 7 by focusing exclusively on the battery, without considering the PCM reservoir. This allows a more localized analysis, making the temperature gradients within the battery more evident due to the better adaptation of the contour scale to the battery temperatures. Once again, it can be observed for both cases that the maximum temperatures are located in the central regions of the battery cell. However, the difference between the temperatures at the top and bottom regions of the cell is now clearly evident in the case of $\phi = 0.20$ [Fig. 8 (b)]. Since the hot liquid PCM accumulates at the top region of the reservoir [Fig. 7 (b)], the temperature gradient between this region and the top of the battery is smaller, reducing the heat dissipation from the battery and, consequently, justifying its higher temperatures at the top. On the other hand, the larger amount of solid PCM at the base of the reservoir results in a greater temperature gradient between this region of the reservoir and the lower regions of the battery, promoting the heat transfer and, consequently, mitigating the temperature increase at the base of the battery. Thus, a high temperature gradient is established in the battery cell, which explains the higher $\Delta T_{cell(max)}$ values observed in Fig. 6 (b) for the case under analysis. A possible solution to prevent the accumulation of hot PCM at the top of the reservoir and promote a more uniform temperature in the battery would be to divide the reservoir into several compartments. This could be achieved using fins, which would also help to improve the heat dissipation from the battery.

4. Conclusions

The objective of this study was to evaluate, using the Constructal Design Method (CDM), the influence of the width (W_{pcm}) of a reservoir filled with PCM on the cooling performance of a Li-ion battery pack; composed of six battery cells connected in a 3s2p configuration; discharged at rates of 3C and 5C. In the context of CDM, the constraint of the system was the battery cell volume (V_{pcm}) ; while the degree of freedom (DoF) was W_{pcm} , which was expressed in dimensionless form by ϕ . The proposed problem was solved computationally through two-dimensional numerical simulations based on the finite volume method (FVM). The mathematical model was multiphase, transient, and based on the conservation equations of mass, energy, and momentum; supplemented by the enthalpy-porosity method to model the PCM melting. Based on the results obtained, the main findings were:

- i) The presence of the PCM reservoir, and consequently its width (W_{pcm}) , has a strong influence on the battery cooling. At the end of the discharge process (SoC \cong 0), the maximum temperature (T_{max}) reached by the battery cell was equal to 53.8°C for the 3C case without the PCM reservoir, followed by 50.8°C for the ϕ = 0.05 case; 44°C for ϕ = 0.10; 42°C for ϕ = 0.15 and 41.8°C for ϕ = 0.20. For the same cases, but considering the 5C discharge rate, T_{max} at SoC \cong 0 were 65°C; 60.3°C; 53.6°C; 52.1°C and 51.9°C, respectively. In other words, the PCM reservoir contributed to the battery cooling, especially when it had a larger width, represented by ϕ .
- ii) In general, T_{max} decreases with ϕ , while the maximum battery cell temperature difference ($\Delta T_{cell(max)}$) increases. However, for values of ϕ greater than 0.15, these variables exhibit an asymptotic behavior, becoming practically constant. Since for $\phi = 0.15$ and 0.20 the volume of the PCM reservoir proved to be larger than necessary. the mass of PCM contained inside it does not melt completely. Thus, the latent heat absorbed by the PCM during its melting becomes practically the same regardless of ϕ , so that T_{max} and $\Delta T_{cell(max)}$ no longer vary as a function of ϕ . Therefore, reducing T_{max} even further and ensuring that $\Delta T_{cell(max)}$ stays below 5°C (the indicated limit) is not done by increasing ϕ . Thus, it can be concluded that the PCM reservoir width (W_{ncm}) significantly contributes to the battery cooling. However, varying this parameter alone is not sufficient to ensure that T_{max} and $\Delta T_{cell(max)}$ remain below the predefined maximum limits considered, which are 40°C and 5°C, respectively. Therefore, solutions that enhance the heat dissipation from the battery and ensure it occurs uniformly are required. One proposed solution, which could be evaluated in future studies, is to divide the PCM reservoir into several partitions using fins. Theoretically, the fins would increase the cooling of the battery and, by dividing the PCM reservoir into several compartments, would prevent the accumulation of molten PCM at high temperatures at the top of the reservoir, thus contributing to the uniform cooling.

Acknowledgement

The authors acknowledge the Brazilian agencies CAPES, CNPq, FAPERGS (Proc. No. 21/2551-0002169-1) and Fundação para a Ciência e Tecnologia, I.P. (doi.org/10.54499/UIDP/04683/2020) for the financial support received. R.S. Borahel has a postdoctoral fellowship funded by FAPERGS. The author G.D. Telli thanks FAPERGS for the financial support (Process: 23/2551-0000802-5). L.A.O. Rocha, L.A. Isoldi and E.D. dos Santos are grant holders of CNPq (Proc. No 307791/2019-0, 309648/2021-1, 308396/2021-9).

References

- [1] Solaymani S. CO2 emissions patterns in 7 top carbon emitter economies: The case of transport sector. Energy, 2019; 168: 989-1001. https://doi.org/10.1016/j.energy.2018.11.145
- [2] Isik M, Sarica K, Ari I. Driving forces of Turkey's transportation sector CO2 emissions: An LMDI approach. Transport Policy, 2020; 97: 210-219. https://doi.org/10.1016/j.tranpol.2020.07.006
- [3] Möring-Martínez G, Senzeybek M, Jochem P. Clustering the European Union electric vehicle markets: A scenario analysis until 2035. Transportation Research Part D: Transport and Environment, 2024; 135: 104372. https://doi.org/10.1016/j.trd.2024.104372
- [4] Barić D, Grabušić S, Jakara M, Emanović M. Reviewing the cost-benefit analysis and multi-criteria decision-making methods for evaluating the effectiveness of lithium-ion batteries in electric vehicles. Sustainability, 2024; 16(1): 233. https://doi.org/10.3390/su16010233
- [5] Saw LH, Poon HM, San Thiam H, Cai Z, Chong WT, Pambudi NA, King YJ. Novel thermal management system using mist cooling for lithium-ion battery packs, Applied Energy. 2018; 223: 146-158. https://doi.org/10.1016/j.apenergy.2018.04.042
- [6] Wang Y, Chen X, Li C, Yu Y, Zhou G, Wang C, Zhao W. Temperature prediction of lithium-ion battery based on artificial neural network model. Applied Thermal Engineering, 2023; 228: 120482. https://doi.org/10.1016/j.applthermaleng.2023.120482
- [7] Pesaran AA. Battery thermal models for hybrid vehicle simulations. Journal of Power Sources, 2002; 110 (2): 377-382. https://doi.org/10.1016/S0378-7753(02)00200-8
- [8] Moaveni A, Siavashi M, Mousavi S. Passive and hybrid battery thermal management system by cooling flow control, employing nano-PCM, fins, and metal foam. Energy, 2024; 288: 129809. https://doi.org/10.1016/j.energy.2023.129809
- [9] Li K, Yao X, Li Z, Gao T, Zhang W, Liao Z, Xu C. Thermal management of Li-ion batteries with passive thermal regulators based on composite PCM materials. Journal of Energy Storage, 2024; 89: 111661. https://doi.org/10.1016/j.est.2024.111661
- [10] Son YW, Kang D, Kim J. Passive battery thermal management system for an unmanned aerial vehicle using a tetrahedral lattice porous plate. Applied Thermal Engineering, 2023; 225: 120186. https://doi.org/10.1016/j.applthermaleng.2023.120186
- [11] Srivastava G, Nandan R, Das MK. Thermal runaway management of Li-ion battery using PCM: A parametric study. Energy Conversion and Management: X, 2022; 16: 100306. https://doi.org/10.1016/j.ecmx.2022.100306
- [12] Alghassab MA. Investigating the performance improvement of lithium-ion battery cooling process using copper fins and phase change materials (PCMs). Case Studies in Thermal Engineering, 2024; 59: 104473. https://doi.org/10.1016/j.csite.2024.104473
- [13] Bejan A, Lorente S. Constructal theory of generation of configuration in nature and engineering. Journal of Applied Physics, 2006; 100: 1-11. https://doi.org/10.1063/1.2221896
- [14] Bejan A, Lorente S. Design with Constructal Theory. John Wiley & Sons Inc, New Jersey, USA, 2008. https://doi.org/10.1002/9780470432709
- [15] Bejan A. The Physics of Life: The Evolution of Everything. St. Martin's Press, New York, USA, 2016.
- [16] Lorenzini G, Rocha LAO. Constructal design of Y-shaped assembly of fins. International Journal of Heat and Mass Transfer, 2006; 49 (23-24): 4552-4557. https://doi.org/10.1016/j.ijheatmasstransfer.2006.05.019
- [17] Borahel RDS, Zinani FSF, Rocha LAO, dos Santos ED, Isoldi LA, Biserni C. Geometric optimization of a rectangular isothermal block inside a lid-driven cavity by means of constructal design. International Communications in Heat and Mass Transfer, 2022; 139: 106499. https://doi.org/10.1016/j.icheatmasstransfer.2022.106499

- [18] Cunegatto EHT, Zinani FSF, Biserni C, Rocha LAO. Constructal design of passive micromixers with multiple obstacles via computational fluid dynamics. International Journal of Heat and Mass Transfer, 2023; 215: 124519. https://doi.org/10.1016/j.ijheatmasstransfer.2023.124519
- [19] Borahel RDS, Zinani FSF, Isoldi LA, dos Santos ED, Rocha LAO. Analysis of the design of cavities with isothermal blocks under mixed convection. Journal of Applied and Computational Mechanics, 2024.
- [20] Cunegatto EHT, Gotardo M, Zinani FSF. Numerical analysis of tube arrangements with one, two, and four degrees of freedom for heat transfer with pseudoplastic fluids. International Journal of Heat and Mass Transfer, 2023; 208: 124080. https://doi.org/10.1016/j.ijheatmasstransfer.2023.124080
- [21] Gungor S, Cetkin E, Lorente S. Thermal and electrical characterization of an electric vehicle battery cell, an experimental investigation. Applied Thermal Engineering, 2022; 212: 118530. https://doi.org/10.1016/j.applthermaleng.2022.118530
- [22] Yang X, Gao X, Zhang F, Luo W, Duan Y. Experimental study on temperature difference between the interior and surface of Li [Ni1/3Co1/3Mn1/3] 02 prismatic lithium-ion batteries at natural convection and adiabatic condition. Applied Thermal Engineering, 2021; 190: 116746. https://doi.org/10.1016/j.applthermaleng.2021.116746
- [23] ANSYS Fluent. Theory Guide. 2023.
- [24] Rubitherm Technologies GmbH. Data Sheet RT28HC. 2024.
- [25] Hariss M, Gounni A, El Alami M. Impact of innovative fin design on phase change material melting for thermal energy storage system. Applied Thermal Engineering, 2023; 231: 120914. https://doi.org/10.1016/j.applthermaleng.2023.120914
- [26] Telli GD, Gungor S, Lorente S. Counterflow canopy-to-canopy and U-turn liquid cooling solutions for battery modules in stationary Battery Energy Storage Systems. Applied Thermal Engineering, 2024; 238: 121997. https://doi.org/10.1016/j.applthermaleng.2023.121997
- [27] Borahel RDS, Telli GD, Bolzoni AA, Rocha LAO, dos Santos ED, Isoldi LA. Numerical analysis of the volumetric heating of a lithium-ion battery pack: an alternative approach. Proceedings of the 20th Brazilian Congress of Thermal Sciences and Engineering (ENCIT), Foz do Iguaçu, Brazil, November, 2024.
- [28] Chen M, Rincon-Mora GA. Accurate Electrical Battery Model Capable of Predicting Runtime and IV Performance. IEEE Transactions on Energy Conversion, 2006; 21(2): 504-511. https://doi.org/10.1109/TEC.2006.874229
- [29] Gungor S, Telli GD, Lorente S. Characterizing Li-ion battery thermal behavior; a methodology when little information is available. International Communications in Heat and Mass Transfer, 2023; 148: 107076. https://doi.org/10.1016/j.icheatmasstransfer.2023.107076
- [30] Voller VR, Prakash C. A fixed grid numerical modelling methodology for convection-diffusion mushy region phase-change problems. International Journal of Heat and Mass Transfer, 1987; 30(8): 1709-1719. https://doi.org/10.1016/0017-9310(87)90317-6
- [31] Yusuf A, Ballikaya S. Performance analysis of concentrated photovoltaic systems using thermoelectric module with phase change material. Journal of Energy Storage, 2023; 59: 106544. https://doi.org/10.1016/j.est.2022.106544
- [32] Roache PJ. Verification and Validation in Computational Science and Engineering, Hermosa, Albuquerque, USA, 1998.
- [33] Celik IB, Ghia U, Roache PJ, Freitas CJ, Coleman H, Raad PE. Procedure for estimation and reporting of uncertainty due to discretization in CFD applications. Journal of Fluids Engineering, 2008; 130. https://doi.org/10.1115/1.2960953
- [34] Ma S, Jiang M, Tao P, Song C, Wu J, Wang J, Deng T, Shang W. Temperature Effect and Thermal Impact in Lithium-Ion Batteries: A Review, Progress in Natural Science: Materials International, 2018; 28(6): 653-666. https://doi.org/10.1016/j.pnsc.2018.11.002